

Measurement and interpretation of ^{-58}Ni elastic scattering from 27 to 49 MeV

Autor(en): **Kiebele, U. / Baumgartner, E. / Gubler, H.P.**

Objekttyp: **Article**

Zeitschrift: **Helvetica Physica Acta**

Band (Jahr): **51 (1978)**

Heft 5-6

PDF erstellt am: **26.04.2024**

Persistenter Link: <https://doi.org/10.5169/seals-114970>

Nutzungsbedingungen

Die ETH-Bibliothek ist Anbieterin der digitalisierten Zeitschriften. Sie besitzt keine Urheberrechte an den Inhalten der Zeitschriften. Die Rechte liegen in der Regel bei den Herausgebern.

Die auf der Plattform e-periodica veröffentlichten Dokumente stehen für nicht-kommerzielle Zwecke in Lehre und Forschung sowie für die private Nutzung frei zur Verfügung. Einzelne Dateien oder Ausdrucke aus diesem Angebot können zusammen mit diesen Nutzungsbedingungen und den korrekten Herkunftsbezeichnungen weitergegeben werden.

Das Veröffentlichen von Bildern in Print- und Online-Publikationen ist nur mit vorheriger Genehmigung der Rechteinhaber erlaubt. Die systematische Speicherung von Teilen des elektronischen Angebots auf anderen Servern bedarf ebenfalls des schriftlichen Einverständnisses der Rechteinhaber.

Haftungsausschluss

Alle Angaben erfolgen ohne Gewähr für Vollständigkeit oder Richtigkeit. Es wird keine Haftung übernommen für Schäden durch die Verwendung von Informationen aus diesem Online-Angebot oder durch das Fehlen von Informationen. Dies gilt auch für Inhalte Dritter, die über dieses Angebot zugänglich sind.

Measurement and interpretation of α - ^{58}Ni elastic scattering from 27 to 49 MeV¹⁾

by U. Kiebele,²⁾ E. Baumgartner, H. P. Gubler, H. O. Meyer,³⁾ G. R. Plattner and I. Sick

Institut für Physik, Universität Basel, CH-4056 Basel, Switzerland

(2. X. 1978)

Abstract. The cross section for elastic scattering of α particles from ^{58}Ni was measured from 27 to 49 MeV in steps of 1 MeV. Data were taken for $120^\circ \leq \theta \leq 172^\circ$. At 37, 43 and 49 MeV complete angular distributions were measured. A thorough analysis in the framework of the optical model shows that neither Woods-Saxon potentials nor 'Regge-pole' descriptions as proposed in the literature are adequate to interpret our data. However, the measurements are well reproduced by a folding potential for the real part of the optical potential, together with a phenomenological volume and surface absorption term.

1. Introduction

In the past, elastic scattering of α particles from various nuclei in the energy range from ~ 10 to 50 MeV has been investigated thoroughly. Usually, the forward angle cross sections can be well described by an optical model, while for backward angles severe discrepancies appear between standard optical model calculations and the measured cross sections. The enhancement of the cross sections in the backward region, especially prominent for some nuclei near $A = 40$, and the pronounced oscillatory structure of the cross section $\sigma(\theta)$ as a function of θ in the backangle region have become known as 'Anomalous Large Angle Scattering' (ALAS) [1–5].

This phenomenon has led to the proposal of several new interaction mechanisms, such as α -clustering in the target nucleus, quasi-molecular states and l -dependent potentials [5–8]. A similar description which introduces so-called 'Regge-poles' into the scattering amplitude [9] also has been used. These theoretical ideas all implicitly involve resonances in the $\alpha +$ nucleus system. If the mechanisms mentioned above really exist, it should be possible to locate these resonant states. A possible experimental verification of their existence is the measurement of excitation functions at many different backward angles. Such a study is described in the present paper.

Since α scattering from ^{58}Ni is not 'anomalous' according to the definition of Eck [5], we decided to start our investigation with ^{58}Ni as a target nucleus. In spite of the 'normal' behaviour of α - ^{58}Ni scattering, traditional analyses, i.e. in the framework of the smooth-cutoff model or of the Woods-Saxon shaped optical potential cannot

¹⁾ Work supported by the Swiss National Science Foundation.

²⁾ Present address: SIN, CH-5234 Villigen.

³⁾ Present address: Physics Dept., Indiana University, Bloomington, Ind. 47401, USA.

explain $\sigma(\theta)$ satisfactorily. We therefore attempted to interpret the data in terms of the same models proposed for the explanation of ALAS.

We show that a satisfactory description of the α - ^{58}Ni angular distributions is obtained when an optical potential resulting from a folding calculation is used. The same conclusion was reached for α - ^{40}Ca , the most notorious case of ALAS, which we investigated in parallel [10] to the present work.

2. Experiment

Angular distributions of elastic α scattering differential cross sections have been measured at the injector cyclotron of SIN. Beam intensities between 400 and 800 nA of $^4\text{He}^{++}$ were obtained using the beam transport system in a non-dispersive mode, resulting in an energy spread of about 100 keV. The beam spot on the target was 2 mm wide and 3 mm high. We used a 1.2 m scattering chamber, containing a target ladder for four targets and two arms carrying the detectors. Detector angles were determined with an accuracy of 0.1° .

The beam current was integrated using a 'split' Faraday cup divided into four sectors. Centering the beam at the location of the Faraday cup and at the target allowed to align the beam axis parallel to the geometrical axis to within 0.2° .

As target we used a rolled nickel foil, with an isotopic purity of 99.96% ^{58}Ni . The target thickness of 1.08 mg/cm^2 contributed at most 350 keV to the energy resolution for backward angles.

The scattered α particles were detected with silicon surface barrier detectors and position-sensitive ion-implanted detectors. At forward angles, three detectors mounted 10° apart from each other were employed, while at backward angles we used two position-sensitive detectors, each covering an angular range of 11.5° . A single detector at 159° provided a control measurement of accumulated charge times target thickness. The angular resolution of the detector systems was $\pm 0.4^\circ$. Thus the solid angles corresponding to one data point were 6.5 msr and 4 msr for the single detectors and the position-sensitive detectors, respectively. This angular resolution gave a contribution of less than 80 keV to the overall energy resolution.

To process the signals from the position-sensitive detectors, an analog divider was used. Energy and position signals were stored as a two-dimensional spectrum on the PDP-11/45 on-line computer.

Differential cross sections for elastic α scattering as small as $0.2 \mu\text{b/sr}$ were measured. For our experimental setup, this corresponds to 10 elastically scattered α particles/hour in one position channel. Even for these small cross sections it was impossible to use more than 800 nA beam current because of pile-up problems. In the backangle region the ratio of elastically scattered α particles to the total number of charged particles reaching the detector was about $1:10^4$. An investigation of the spectrum with a ΔE - E telescope showed that most of these particles were protons and deuterons, much fewer tritons and α , and only a few ^3He . While these particles led to severe pile-up problems, they did not affect the identification of the elastically scattered α particles. Figure 1 shows a typical spectrum of the particles detected with a 1 mm thick silicon surface barrier detector. The elastic and the first inelastic α peak are well separated, while the second excited state in ^{58}Ni already overlaps with other states.

The results of our measurements are presented in Figures 2–5. Plotted is the cross section for elastic scattering in the c.m. system divided by the Rutherford cross section

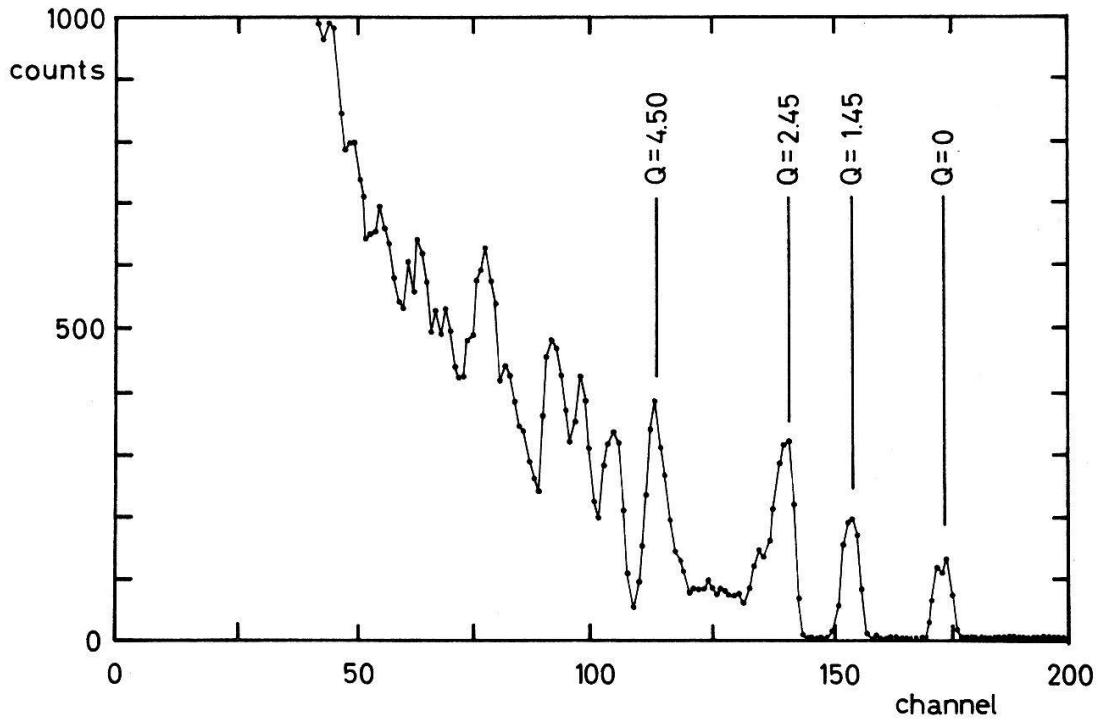


Figure 1

Typical energy spectrum of α particles scattered from ^{58}Ni , with $E_\alpha = 37$ MeV and $\theta_{\text{lab}} = 159^\circ$. Four prominent states are labelled by their excitation energy (MeV) in ^{58}Ni .

σ_R ,

$$\sigma_R(\vartheta) = 1.29 \left(\frac{Z_\alpha Z_T}{E_{\alpha, \text{lab}} [\text{MeV}]} \right)^2 \cdot \left(\frac{m_\alpha + m_T}{m_T} \right)^2 \cdot \left(\sin \frac{\theta}{2} \right)^{-4} \left[\frac{mb}{sr} \right]. \quad (1)$$

The error bars contain the statistical error only, and they are not shown if smaller than 10%. The absolute normalization of the cross sections has been estimated to be accurate to $\pm 5\%$. Tables of $\sigma(\theta)$ are available from one of the authors upon request.

The error of the measured cross section, as used in the fitting program, not only contains the statistical error, but also the uncertainty of the angle, and it is set to a minimal error of 5%, if all other terms are smaller than this.

3. Data analysis

The differential cross section $\sigma(\theta)$ for elastic scattering is given by the square of the modulus of the scattering amplitude

$$f(\theta) = f_C(\theta) + \frac{1}{2ik} \sum_l (2l+1) e^{2i\sigma_l} (S_l - 1) P_l(\cos \theta). \quad (2)$$

Here $f_C(\theta)$ is the point Coulomb amplitude, S_l the S -matrix element, σ_l the Coulomb phases and P_l Legendre polynomials.

For the elastic scattering of strongly absorbed particles one can obtain a first approximation to the true scattering amplitude by phenomenologically parametrizing the S -matrix elements S_l , as in the so-called sharp-cutoff [11] or the smooth-cutoff [6, 12, 13] models.

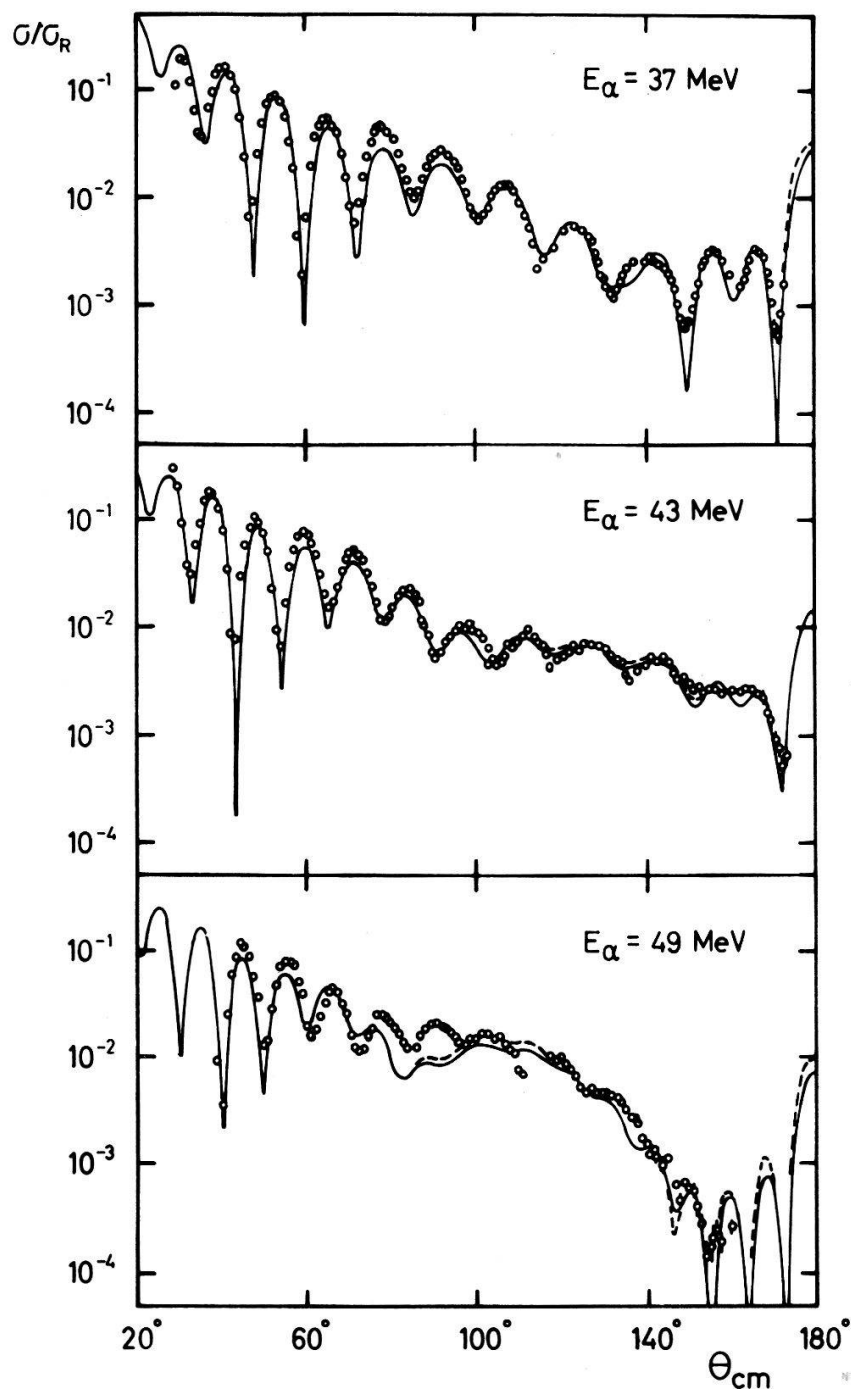


Figure 2

Differential cross section for α particles elastically scattered from ^{58}Ni . Error bars are shown only for statistical errors greater than 10%. The solid (dashed) curves correspond to fit I (fit II) of Table 3.

A more physical parameterization consists in describing the α -nucleus interaction by a complex potential $U(r)$. To calculate the values of the S -matrix, a one-dimensional Schrödinger equation has to be solved. $U(r)$ can be parametrized freely (phenomenological approach), or by using a folding potential [10, 14–17] extracted from a microscopic model of the α nucleon interaction. This latter parameterization is more satisfactory, because the potential is derived from physically meaningful parameters, e.g. from the nucleon distribution and the measured α -nucleon interaction. While the

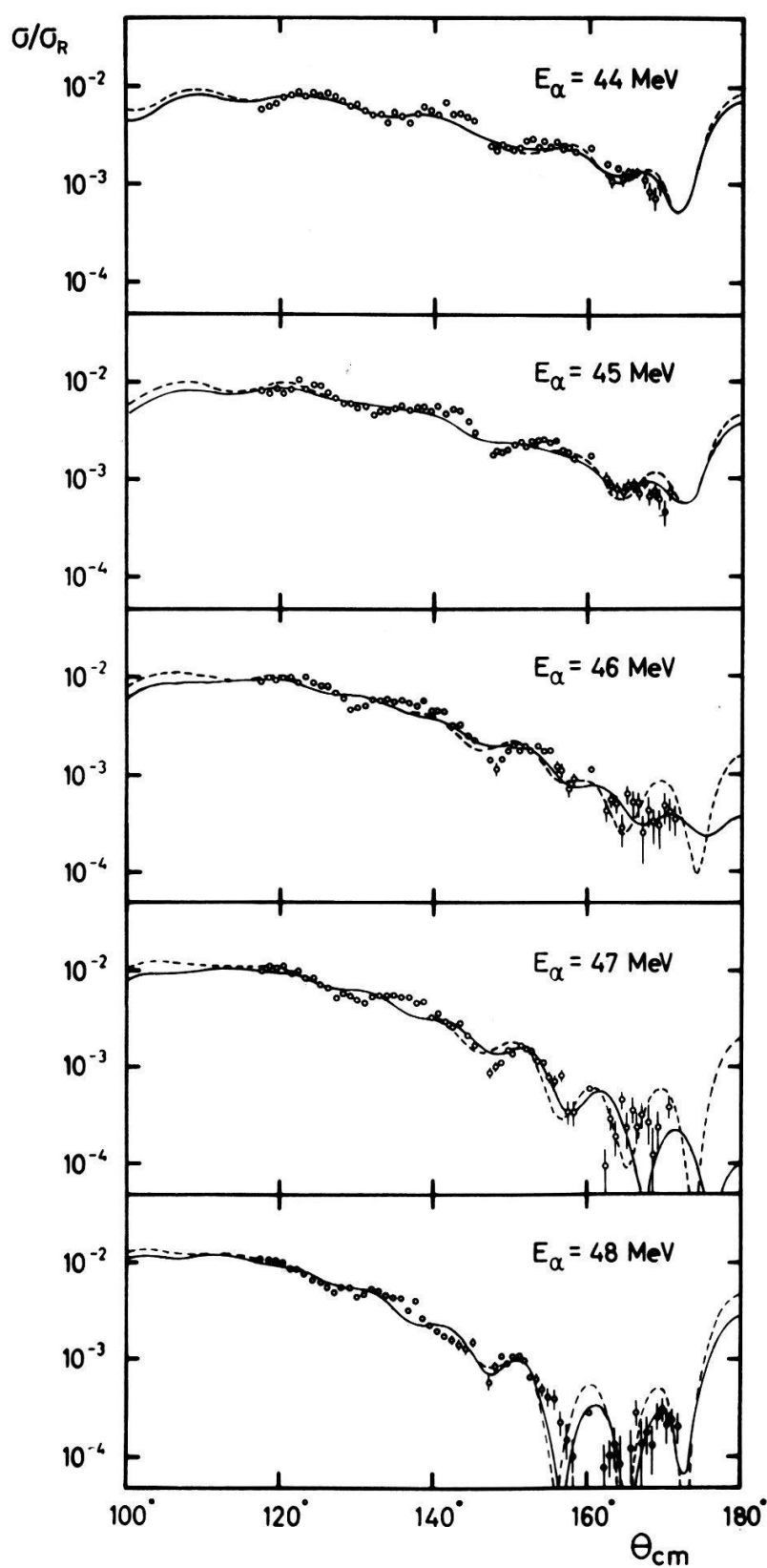


Figure 3
Differential cross section for α particles elastically scattered from ^{58}Ni . The solid (dashed) curves correspond to fit I (fit II).

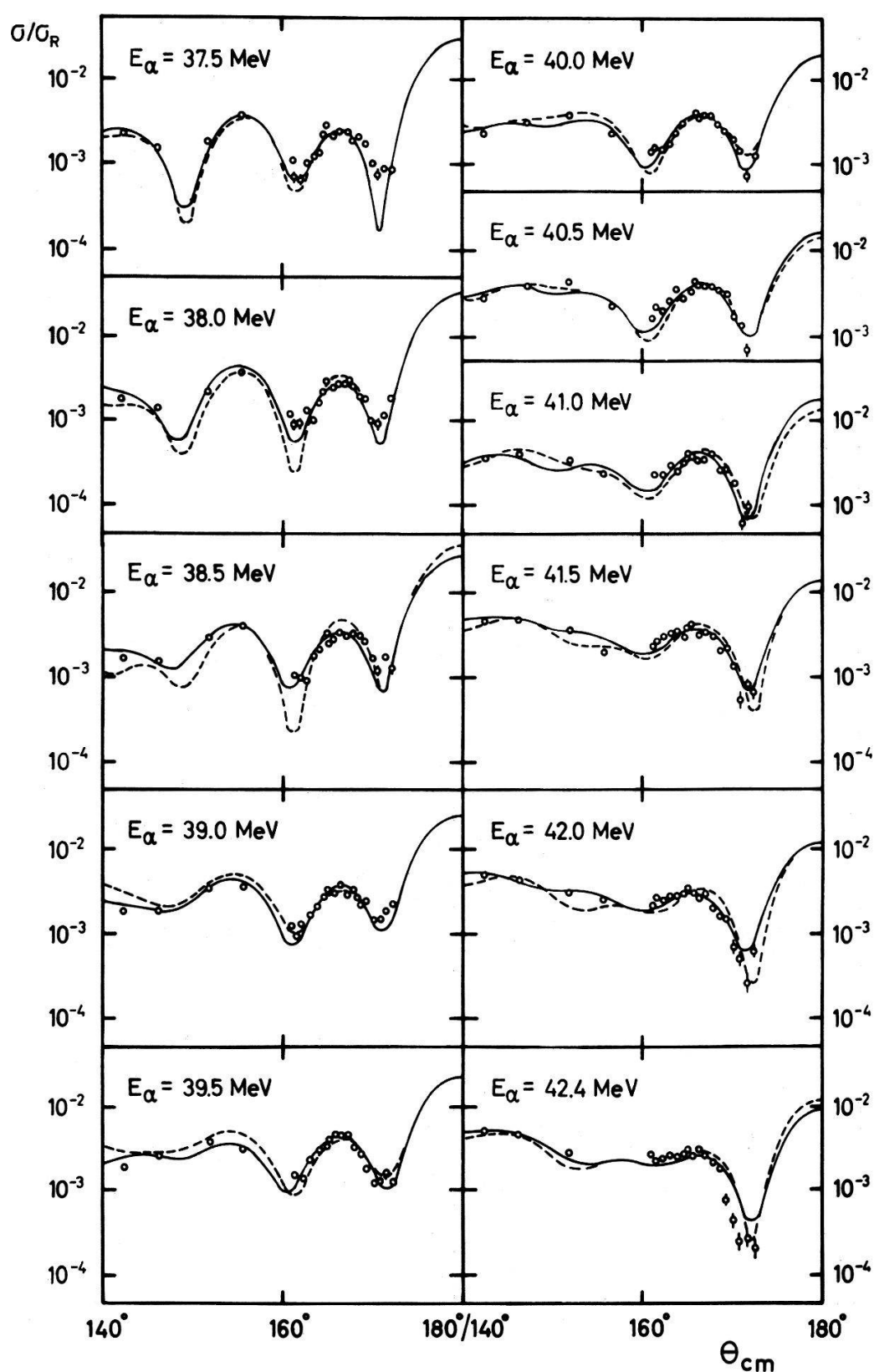


Figure 4

Differential cross section for α particles elastically scattered from ^{58}Ni . The solid (dashed) curves correspond to fit I (fit II).

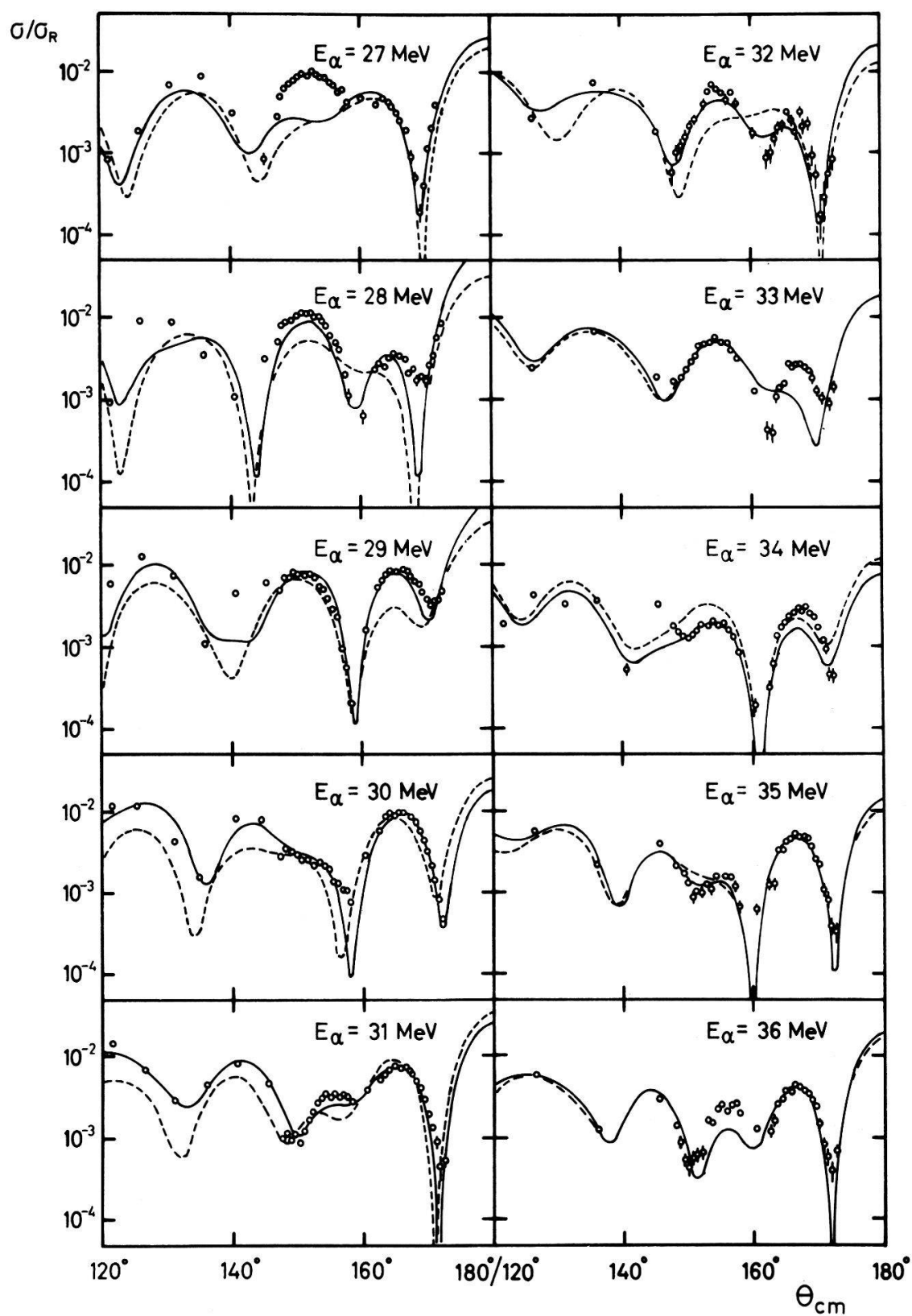


Figure 5
Differential cross section for α particles elastically scattered from ^{58}Ni . The solid (dashed) curves correspond to fit I (fit II).

real part of the potential can be calculated by this model, the imaginary part can only be estimated [14], at least in the energy region covered in this work.

In this section, we present the interpretation of our data with these various models. The goal of these attempts is to see whether any of these reaction mechanisms allows a systematic description of the α - ^{58}Ni elastic cross section as a function of energy.

3.1 Smooth-cutoff model

A simple model for α scattering, the sharp-cutoff model [11], is too stringent a parametrization of S_l . Even a generalization, the smooth-cutoff representation [6, 12, 13], where the S -matrix elements are taken to be

$$S_l = B(l) = (1 + e^{-i\alpha} e^{(L-l)/\Delta})^{-1}, \quad (3)$$

is known to describe the data only qualitatively.

Here L is the cutoff angular momentum, Δ describes the diffuseness of the cutoff, and α is a free phase introduced to allow for complex values of S_l .

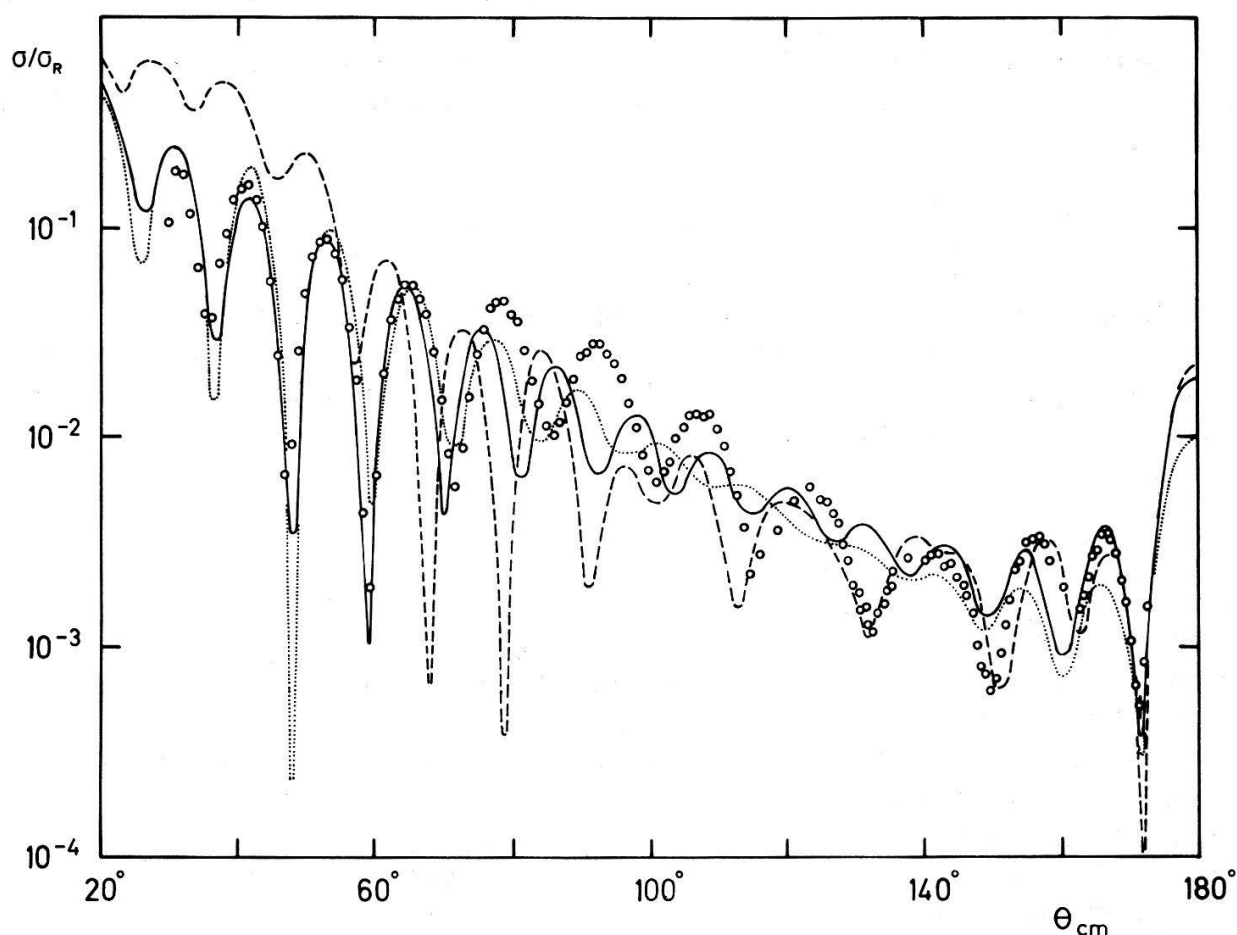


Figure 6
'Smooth-cutoff plus Regge-pole' fits to the angular distribution at $E_\alpha = 37$ MeV. The solid curve is a 'smooth-cutoff' fit to the data for $\theta < 70^\circ$ (fit 3 of Table 1). The dashed curve is a 'smooth-cutoff plus Regge-pole' fit for $\theta > 120^\circ$ (fit 2), and the dotted curve is a 'smooth-cutoff plus Regge-pole' fit to the whole angular distribution (fit 1).

Astonishingly, when fitting the forward angle data only, this model predicts a roughly correct pattern for the backward cross sections. As an example, the solid line in Figure 6 represents a fit to the 37 MeV data for $\theta < 70^\circ$. This fit not only describes the data for $\theta < 70^\circ$, but also for $\theta > 140^\circ$ rather well. However, it fails in the intermediate angle region. This behaviour occurs also at other energies than 37 MeV, although the back-angle agreement is not always as striking as in this case.

3.2. Smooth-cutoff model plus Regge-pole

The fact [1] that the back-angle cross section of 'anomalous' α - ^{40}Ca scattering is proportional to $|P_{l_0}(\cos \theta)|^2$ with one single l_0 , which depends on the bombarding energy, suggested the introduction of 'Regge-poles', i.e. poles or 'resonances' in the complex l -plane. If there are quasi-molecular or rotational states in the intermediate nucleus, which strongly decay into the elastic channel, they might be described by such resonances in l . All other contributions to elastic scattering must be accounted for by choosing a suitable background.

Such a parametrization of S_l was used by Gruhn [1]. Since the smooth-cutoff representation of Blair [12, 13] could not describe the whole angular distribution, S_l was chosen as the S_l from the smooth-cutoff model plus a δ -function in l , emphasizing a particular angular momentum.

In the present work, the S -matrix elements S_l are taken as a background term $B(l)$ of the form of equation (3) in the smooth-cutoff representation multiplied by a 'Regge-pole' factor:

$$S_l = B(l) \frac{l - L_0 - iz(l)}{l - L_0 - ip(l)} = B(l) \left(1 + \frac{iD(l)}{l - L_0 - (i/2)\Gamma(l)} \right). \quad (4)$$

The Regge-pole factor [6] describes a resonance in l , where $p(l)$ and $z(l)$ give the pole and the zero position in the complex l -plane. The resonance is centered at L_0 with a total width Γ . The l -dependence of D and Γ is adopted to be the same as the l -dependence of the background term itself, i.e.

$$D(l) = D(1 + e^{(l-L)/\Delta})^{-1}, \quad (5)$$

$$\Gamma(l) = \Gamma(1 + e^{(l-L)/\Delta})^{-1}. \quad (6)$$

From past experience, one does not expect to find a good representation of the cross sections in terms of the smooth-cutoff plus Regge-pole model. Nevertheless, we have tried to fit our data at various energies using this descriptions, since it is a simple parameterization, that allows a sensitive test for l -dependent effects. We have not found satisfactory fits for the whole angular distribution at any energy. Only the extreme forward and backward region can be well represented. Most discrepancies between experiment and calculation occur in an intermediate angle region from about 80° to 140° . As an example, in Figure 6 a calculation is shown for 37 MeV. The corresponding parameters are given in Table 1. The dotted curve is a fit to the whole angular distribution, while the dashed curve represents a fit using data with $\theta > 120^\circ$, only. Apparently, the Regge-pole, while improving the fit in the backward region, leads to a bad representation of the forward angle data.

Fits to backward angle data show only a small systematic energy dependence of the parameters in the sense that L and L_0 follow more or less the appropriate l for the

Table 1
 'Smooth-cutoff plus Regge-pole' fits to the angular distribution at $E_\alpha = 37$ MeV. The corresponding curves are shown in Figure 6. Parameter definitions according to equations 3–6.

	Angular region of fit	α	L	Δ	D	$\hat{\Gamma}$	L_0	χ^2/n of fit	χ^2/n of whole angular distribution
1	All angles	-0.9345	13.08	1.914	13.29	20.00	13.23	33.22	33.22
2	$\theta > 120^\circ$	-1.571	13.43	2.979	3.08	15.24	16.38	11.28	367.8
3	$\theta < 70^\circ$	1.196	15.57	0.902	—	—	—	12.10	49.55

grazing collision, where $lh = kr$. Here r is the sum of the α and the ^{58}Ni radii. Since the parameters show strong fluctuations as a function of energy, and since they can not describe the intermediate angle behaviour correctly, we conclude that *the smooth-cutoff plus Regge-pole model is not adequate* for reproducing α scattering from ^{58}Ni .

3.3. Woods-Saxon potential

Instead of choosing a phenomenological parametrization of the S -matrix, S_l can be calculated in the framework of the optical model. Commonly, the radial dependence of the optical potential is taken to be of the Woods-Saxon form. In the past the optical model in this representation has been very successful e.g. for the description of proton scattering from elements throughout the periodic table [18]. However, one should not forget that initially the Woods-Saxon potential was chosen for its numerically convenient form. It is therefore not surprising, that there are cases where this special form of $U(r)$ turns out to be inadequate [10].

The optical potential in the Woods-Saxon parametrization is

$$U(r) = V_C - Vf(x_0) - i \cdot \left[Wf(x_w) - 4W_D \cdot \frac{d}{dx_D} f(x_D) \right], \quad (7)$$

with V_C the Coulomb potential of a uniformly charged sphere with $R_C = r_C \cdot A^{1/3}$ and

$$f(x_i) = \frac{1}{1 + e^{x_i}}, \quad (8)$$

$$x_i = \frac{r - r_i \cdot A^{1/3}}{a_i}. \quad (9)$$

In the past, many analyses of elastic scattering have been carried out in the framework of this model. Often, different families of potentials give equivalent fits to the data (ambiguities), since they lead to nearly the same S -matrix elements [18–24]. As an example, Figure 7 shows fits to the 37 MeV data corresponding to four completely different sets of potential parameters (see Table 2). Figure 7 by no means represents a complete collection of ambiguities. Systematic searches [19] show several nearly equivalent minima in χ^2 , and we have found about a dozen sets yielding acceptable fits to a given angular distribution.

It is easy to find an optical potential that explains an individual angular distribution, at least for energies below 43 MeV. However, it has not been possible to

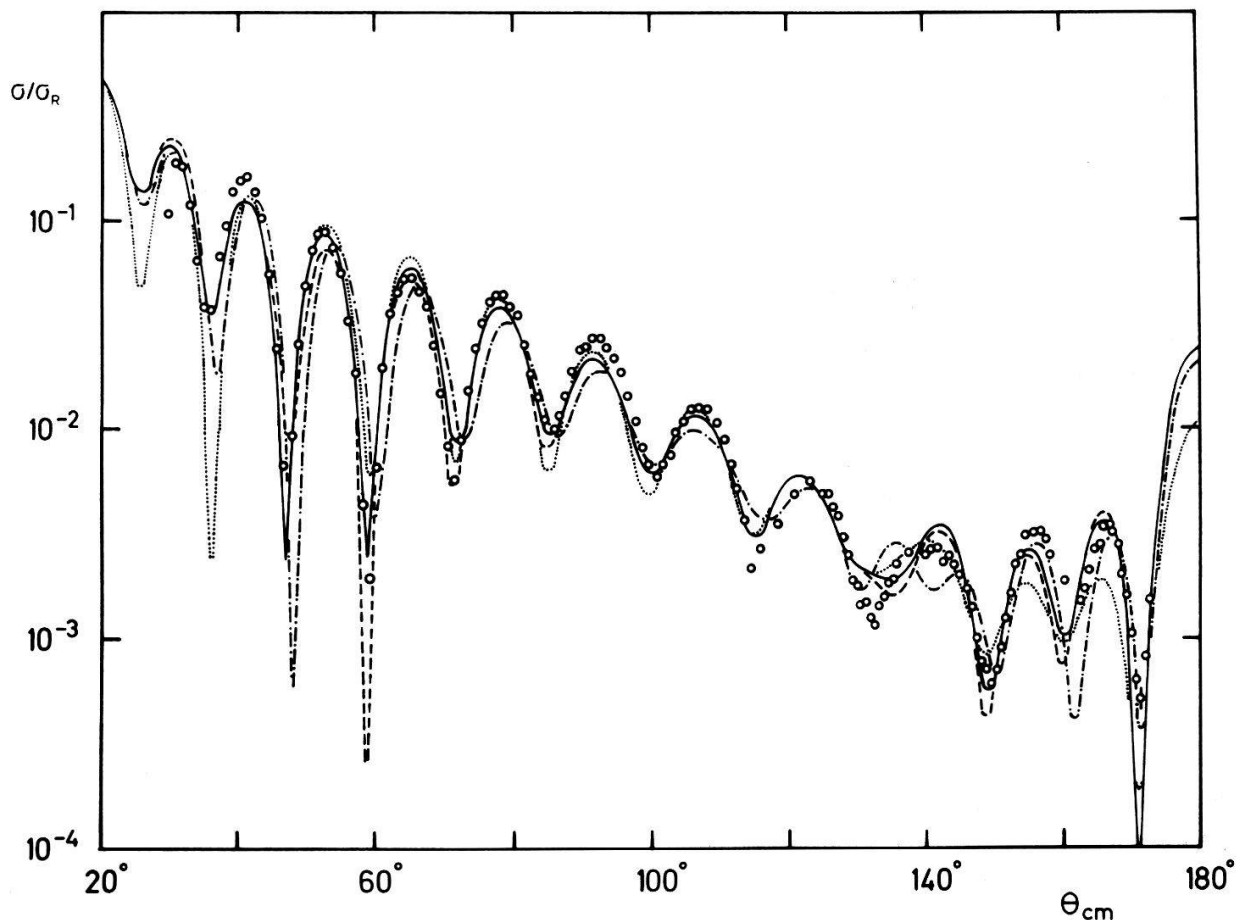


Figure 7
Ambiguities of Woods-Saxon shaped optical potentials fitted to the angular distribution at $E_\alpha = 37$ MeV. The curves correspond to the parameter set 1 (.....), set 2 (—), set 3 (---) and set 4 (-.-.-) of Table 2.

find a weakly energy dependent Woods-Saxon potential for the whole energy region from 27 to 49 MeV. Starting with potential 2 of Table 2, we have found fairly good fits for all of the data between 35 and 40 MeV and also for some energies below 35 MeV, but the parameters are not smoothly energy dependent, varying up to 50% of their average value. Moreover, it has been impossible to get acceptable fits for the data above 40 MeV with any parameter set we tried. Any potential describing the forward or intermediate angle data in the region above 40 MeV always predicts a strong oscillatory backward enhancement, in contradiction to experiment.

Table 2
Ambiguities of Woods-Saxon shaped optical potentials fitted to the angular distribution at $E_\alpha = 37$ MeV. Parameter definitions according to equations 7–9.

	V	r_0	a_0	W	r_W	a_W	r_C	χ^2/n
1	15.29	1.761	0.5878	25.96	1.390	0.5599	1.40	7.56
2	62.41	1.541	0.5654	13.07	1.617	0.4000	1.40	4.31
3	97.77	1.483	0.5458	16.47	1.561	0.4000	1.40	5.43
4	142.0	1.366	0.5825	33.31	1.292	0.4576	1.40	9.97
5	226.9	1.213	0.6915	24.83	1.518	0.4619	1.40	25.77

3.4. Woods-Saxon potential plus Regge-pole

Although Regge-poles or similar l -dependent terms were introduced first to improve the smooth-cutoff model [1, 6], their use is not restricted to this particular model. One can also try to improve the Woods-Saxon optical model by introducing a Regge-pole. Such a description would be convenient to represent 'molecular' states or resonances with a well defined l . Although the optical model itself can be understood as a superposition of many Regge-poles, the introduction of an additional pole emphasizes the influence of one specific partial wave without changing the average optical potential.

In our study, successful fits using this model in general have lead to a Regge-pole factor with L_0 near grazing angular momentum. Below 40 MeV, the new parameter sets (with 10 free parameters instead of 6) have given fits with χ^2 about half as large as the one for a pure Woods-Saxon optical potential. Yet, the variation of the parameters with energy has stayed as large as before. Also, it still has been impossible to extend the description beyond 40 MeV.

3.5. Generalized potentials and the folding model

Since a detailed understanding of α scattering with a systematic energy dependence is difficult, we can try to learn something about the potential by investigating only the characteristic features of angular distributions such as the positions of cross section maxima in the angle-energy plane. Taking a fixed optical potential describing one of the angular distributions, we have systematically varied one parameter at a time to study the behaviour of the maxima and compare it with the experimental pattern. This investigation has shown, that the position of the diffraction pattern in the forward region as well as the position of the very backward maxima depends almost exclusively on the real part of the potential. In addition we have found that the imaginary potential very strongly influences the intermediate angle region; it determines the angular region where the forward fall-off changes into the backangle enhancement, and it determines the width of the interference region. The deeper the imaginary potential, or the larger the radius of the imaginary potential, the more the backward structure vanishes. A stronger imaginary potential shifts the interference region to larger angles and suppresses the enhancement of the back-angle oscillations.

Our study has shown, that a potential can qualitatively describe the position of the cross section maxima in a whole angle-energy region, even though it does not give the correct magnitude of the cross section. Suitable combinations of real and imaginary potentials also allow to produce a backward enhancement of σ/σ_R , *without introducing any special reaction mechanism*.

Given this situation, it seems promising to investigate more general shapes of $V(r)$. One possibility to generalize the optical model is to use form factors that are more flexible than the commonly used Woods-Saxon form. The Woods-Saxon form factor of equation (8) may e.g. be modified to

$$f'(x'_i, v) = \left(\frac{1}{1 + e^{x'_i}} \right)^v, \quad (10)$$

$$x'_i = \frac{r - r_i \cdot A^{1/3}}{a_i \cdot v}, \quad (11)$$

thus giving an additional degree of freedom [10, 25]. In several investigations a squared Woods-Saxon form factor ($v = 2$) was adopted [26, 27].

The above model is phenomenological, because v does not have an obvious physical significance. A more fundamental approach is to calculate the real part of the α -nucleus potential using the folding model [10, 14–17]. Following the work of Vinh Mau [14], we use the real part $V(r)$ of the potential

$$V(r) = \int \rho(r') \cdot V_{\alpha N}(r - r') \cdot dr', \quad (12)$$

where $\rho(r)$ is the nucleon point density in the target nucleus. For $V_{\alpha N}$ we use a local potential

$$V_{\alpha N}(r) = -U_0 \cdot (1 - \varepsilon \cdot E_\alpha) \cdot e^{-(r/\mu)^2}, \quad (13)$$

which is a good approximation for the effective α -nucleon interaction [28]. It has been shown that this local potential, owing to its energy dependence, is equivalent to a non-local potential [29] including exchange terms.

We have evaluated the real part of our ^{58}Ni optical potential according to equations (12) and (13). The nucleon density $\rho(r)$ has been taken to be the charge density of Reference 30, unfolded by the charge distribution of the proton, and normalized to the proper number $A = 58$ of nucleons. The corresponding potential is displayed as a solid line in Figure 9. For the imaginary part, we have allowed for volume and surface absorption by admitting phenomenological Woods-Saxon potentials (equation 7). By fitting at seven selected energies (where we had measured complete angular distributions or where we could combine our back-angle data with existing measurements of forward data, see References 22, 23, 31–36) we first obtained a preliminary set of parameters. In these fits we had 7 free parameters, i.e. W , W_D , r_W , r_D , a_W , a_D (equation 7) and the normalization factor g_R of the real part of the potential. The real part was taken as $g_R \cdot V(r)$, where $V(r)$ is the potential calculated from equations (12) and (13). These preliminary fits allowed us to fix the geometry parameters r_W , r_D , a_W and a_D of the imaginary part at average values (see Table 3). It was necessary to use volume and surface absorption, because setting either $W = 0$ or $W_D = 0$ resulted in strong fluctuations of the imaginary part of the potential as a function of energy.

For the best fit of individual energies, we then have varied three parameters (fit I); the geometry parameters were fixed, and only g_R , W and W_D , i.e. the potential depth of the real and the imaginary part were free. The results of fit I are shown as a solid curve in Figures 2–5, the parameters are given in Table 3 and Figure 8. Since the energy dependence of the imaginary potential depths W and W_D from fit I can be approximated by a straight line, we also have tried to fit our data with only one free parameter g_R (fit II). W and W_D were taken to depend linearly on energy, and r_W , r_D ,

Table 3

Folding model potential. Parameter definitions of the imaginary part of the potential correspond to equations 7–9, g_R is the normalization factor of the real folding potential.

	g_R	W	r_W	a_W	W_D	r_D	a_D
I	See Figure 10	See Figure 10	1.39	0.21	See Figure 10	1.20	0.55
II	See Figure 10	$52. - 1. * E_\alpha$	1.39	0.21	$-18.2 + 1.14 * E_\alpha$	1.20	0.55

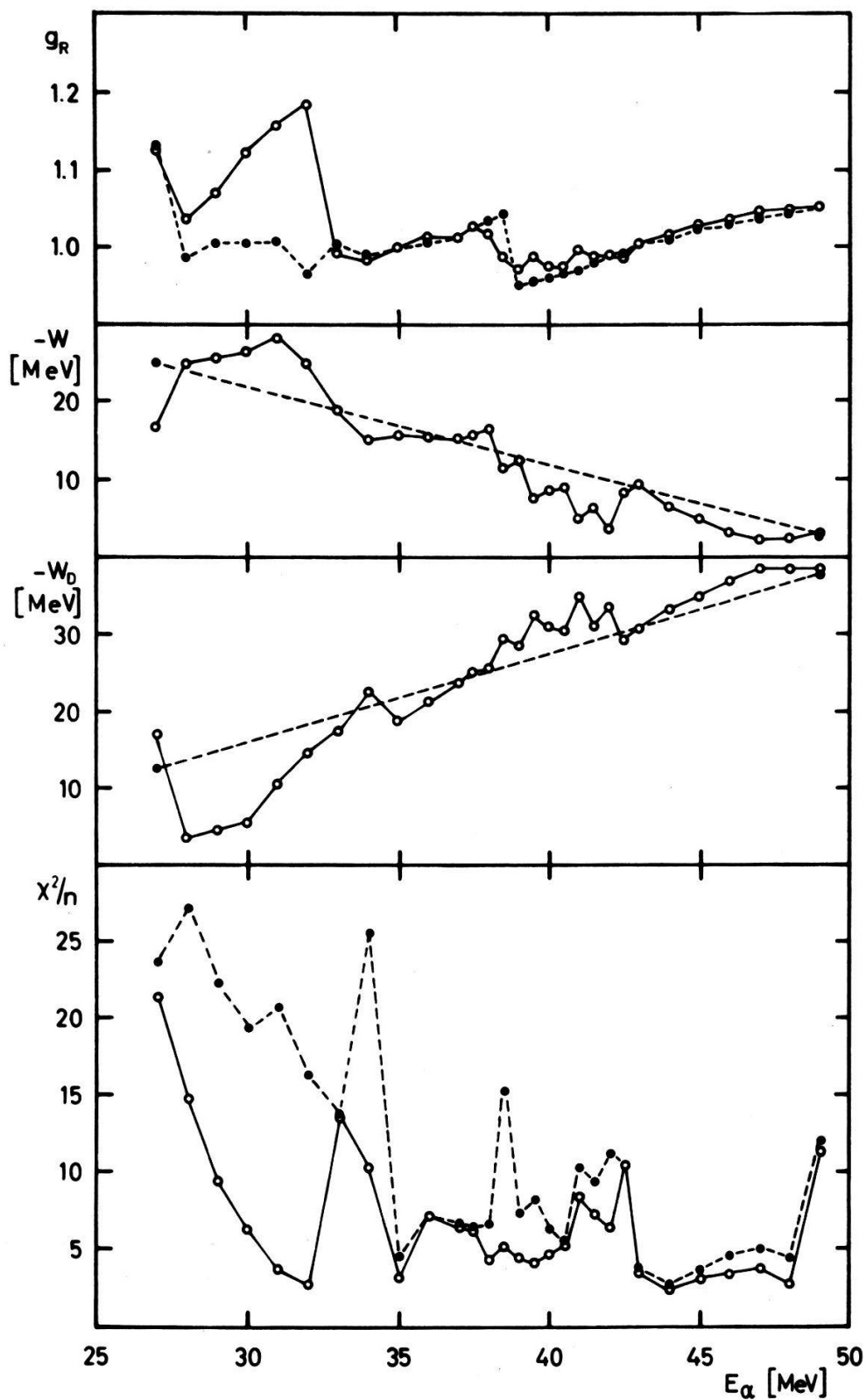


Figure 8

Energy dependence of the parameters of fit I and II. The quantity g_R is the normalization factor of the real folding potential, while W and W_D are the strengths of the imaginary parts of the potential for volume and surface absorption respectively. Open circles (solid line) stand for fit I, solid dots (dashed line) for fit II. The corresponding geometry parameters are given in Table 3. The quality of the fits is also indicated.

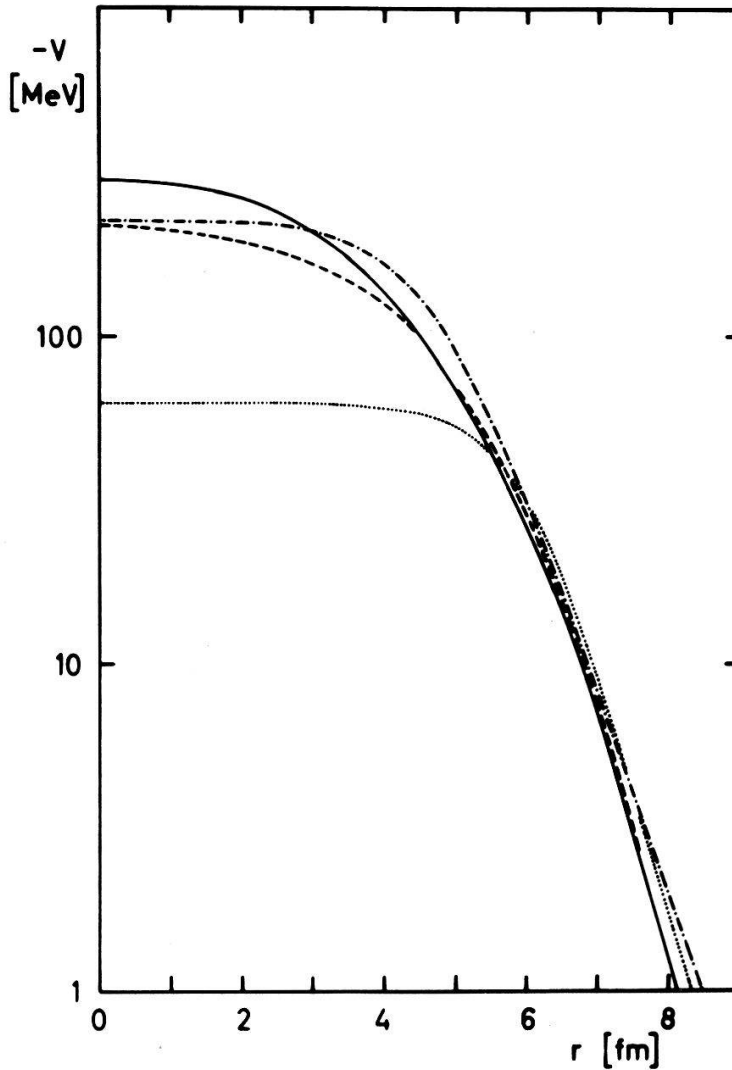


Figure 9

Real part of the optical potential for various models. All potentials were fitted to the 37 MeV angular distribution. The solid curve belongs to the folding model, the dashed curve to a modified Woods-Saxon potential with $V = 221.4$ MeV, $r_0 = 1.58$ fm, $a_0 = 0.42$ fm and $v = 3.15$. As a comparison the two Woods-Saxon potentials 2 (.....) and 5 (-.-.-) from Table 2 are also given.

a_W , a_D were the same as in fit I (see Table 3 and Figure 8). The results of fit II are displayed as the dashed curve in Figures 2–5. Clearly, we can describe our data or at least the position of the cross section maxima fairly well with fit I, or even with fit II, where only one parameter is adjusted.

Modified Woods-Saxon potentials of the form of equations (10) and (11) have a shape quite similar to the one of folding potentials. As an example, we show in Figure 9 the folding potential used in our analysis and the corresponding modified Woods-Saxon potentials, fitted to the same data. We also display a Woods-Saxon potential of similar depth, and the Woods-Saxon potential giving the best fit at this energy. Obviously, all four potentials are quite similar in the surface region. The main difference occurs in the region $r \sim 4$ fm where $V(r)$ has a shoulder. At small radii, the potentials are very different, but this hardly influences $\sigma(\theta)$ because of the strong absorption of α -particles in nuclear matter.

4. Conclusions

Elastic α scattering from ^{58}Ni in the energy region from 27 to 49 MeV shows almost no backward enhancement of $\sigma(\theta)$ when compared to typical cases of ALAS. However, attempts to describe the data with ordinary Woods-Saxon shaped potentials lead to similar problems as in the case of so-called 'anomalous' large angle α scattering. Customarily, 'Regge-poles' or other l -dependent terms have been introduced to explain ALAS. In the case of α - ^{58}Ni scattering such terms improve the quality of the fits to individual angular distributions, but they cannot provide a systematic description over a wide energy range.

This paper shows that the scattering of α particles from ^{58}Ni can be described by the optical model, provided one uses an appropriate radial shape for the real part of the potential. No special mechanisms are then needed to explain the general features of the data. The scattering of α particles in this energy region is very sensitive to the shape of the real potential in the surface region. It turns out, that Woods-Saxon form factors do not have enough flexibility to reproduce the measured cross sections. Adequate potential forms can be found by using modified Woods-Saxon potentials or folding potentials.

After completion of our analysis, a paper on the same topic has been published by Budzanowski et al. [27]. They agree with our conclusions concerning the choice of the correct form factor, namely that a Woods-Saxon shape is not the best potential parametrization for α scattering. However, the potentials resulting from our work differ in detail from the ones found by Budzanowski et al. [27].

There remain several open questions. It is not clear whether the folding model really gives the correct form of the potential. Contributions to elastic scattering from compound processes have not been investigated, but might appear at large angles. Furthermore, the basic problem of understanding the imaginary part of the α -nucleus optical potential, and in particular its strong and erratic A -dependence remains a challenge.

We would like to thank Dr. M. Pauli and the SIN cyclotron staff for their help with this work.

REFERENCES

- [1] C. R. GRUHN and N. S. WALL, Nucl. Phys. *81*, 161 (1966).
- [2] R. STOCK, G. GAUL, R. SANTO, M. BERNAS, B. HARVEY, D. HENDRIE, J. MAHONEY, J. SHERMAN, J. STEYAERT and M. ZISMAN, Phys. Rev. *C6*, 1226 (1972).
- [3] D. AGASSI and N. S. WALL, Phys. Rev. *C7*, 1368 (1973).
- [4] M. B. LEWIS, C. B. FULMER, D. C. HENSLEY, C. C. FOSTER, N. M. O'FALLON, S. A. GRONEMEYER and W. W. EIDSON, Phys. Rev. *C10*, 2441 (1974).
- [5] J. S. ECK, W. J. THOMPSON, K. A. EBERHARD, J. SCHIELE and W. TROMBIK, Nucl. Phys. *A255*, 157 (1975).
- [6] K. W. McVOY, Phys. Rev. *C3*, 1104 (1971).
- [7] R. C. FULLER and K. W. McVOY, Phys. Lett. *55B*, 121 (1975).
- [8] J. T. LONDERGAN and K. W. McVOY, Nucl. Phys. *A201*, 390 (1973).
- [9] T. TAMURA and H. H. WOLTER, Phys. Rev. *C6*, 1976 (1972).
- [10] H. P. GUBLER, U. KIEBELE, H. O. MEYER, G. R. PLATTNER and I. SICK, Phys. Lett. *74B*, 202 (1978).
- [11] J. S. BLAIR, Phys. Rev. *95*, 1218 (1954).
- [12] J. S. BLAIR, D. SHARP and L. WILETS, Phys. Rev. *125*, 1625 (1962).
- [13] J. A. MCINTYRE, K. H. WANG and L. C. BECKER, Phys. Rev. *117*, 1337 (1960).
- [14] N. VINH MAU, Phys. Lett. *71B*, 5 (1977).
- [15] F. MICHEL, Phys. Lett. *60B*, 229 (1976).

- [16] F. MICHEL, *Phys. Rev. C* **13**, 1446 (1976).
- [17] P. MAILANDT, J. S. LILLEY and G. W. GREENLEES, *Phys. Rev. C* **8**, 2189 (1973).
- [18] C. M. PEREY and F. G. PEREY, *Nuclear Data Tables* **17**, 1 (1976).
- [19] I. N. SIMONOV, K. O. TERENETSKII and V. V. TOKAREVSKII, *Sov. J. Nucl. Phys.* **14**, 59 (1972).
- [20] H. H. CHANG, B. W. RIDLEY, T. H. BRAID, T. W. CONLON, E. F. GIBSON and N. S. P. KING, *Nucl. Phys. A* **270**, 413 (1976).
- [21] K. W. KEMPER, A. W. OBST and R. L. WHITE, *Phys. Rev. C* **6**, 2090 (1972).
- [22] A. A. COWLEY, P. M. CRONJE, G. HEYMANN, S. J. MILLS and J. C. VAN STADEN, *Nucl. Phys. A* **229**, 256 (1974).
- [23] C. B. FULMER, J. BENVENISTE and A. C. MITCHELL, *Phys. Rev.* **165**, 1218 (1968).
- [24] D. C. WEISSER, J. S. LILLEY, R. K. HOBBIIE and G. W. GREENLEES, *Phys. Rev. C* **2**, 544 (1970).
- [25] F. MICHEL and R. VANDERPOORTEN, *Phys. Rev. C* **16**, 142 (1977).
- [26] D. A. GOLDBERG, *Phys. Lett.* **55B**, 59 (1975).
- [27] A. BUDZANOWSKI, H. DABROWSKI, L. FREINDL, K. GROTOWSKI, S. MICEK, R. PLANETA, A. STRZALKOWSKI, M. BOSMAN, P. LELEUX, P. MACQ, J. P. MEULDERS and C. PIRART, *Phys. Rev. C* **17**, 951 (1978).
- [28] M. LASSAUT and N. VINH MAU, *Phys. Lett.* **70B**, 14 (1977).
- [29] D. F. JACKSON, R. C. JOHNSON, *Phys. Lett.* **49B**, 249 (1974).
- [30] I. SICK, J. B. BELLICARD, M. BERNHEIM, B. FROIS, M. HUET, PH. LECONTE, J. MOUGEY, PHAN XUAN-HO, D. ROYER and S. TURCK, *Phys. Rev. Lett.* **35**, 910 (1975).
- [31] W. TROMBIK, K. A. EBERHARD, G. HINDERER, H. H. ROSSNER, A. WEIDINGER and J. S. ECK, *Phys. Rev. C* **9**, 1813 (1974).
- [32] M. INOUE, *Nucl. Phys. A* **119**, 449 (1968).
- [33] H. W. BROEK, J. L. YNTEMA, B. BUCK and G. R. SATCHLER, *Nucl. Phys.* **64**, 259 (1965).
- [34] D. K. MCDANIELS, J. S. BLAIR, S. W. CHEN and G. W. FARWELL, *Nucl. Phys.* **17**, 614 (1960).
- [35] O. N. JARVIS, B. G. HARVEY, D. L. HENDRIE and J. MAHONEY, *Nucl. Phys. A* **102**, 625 (1967).
- [36] I. KUMABE, H. OGATA, M. INOUE, Y. OKUMA and J. MUTO, *J. Phys. Soc. Japan* **19**, 147 (1964).